

Controllable growth of ZnO nanostructures by hydrothermal method

H.K. Ghaydar^a, S. Jamehbozorgi^{*a}, A. Mahmoudi^b, S. Dehghanpour^c

^aDepartment of Chemistry, Islamic Azad University, Arak Branch, Arak, Iran

^bFaculty of Chemistry, Islamic Azad University, Tehran North Branch, Tehran, Iran

^cFaculty of Chemistry, Alzahra University, Vanak, Tehran, Iran

Received August 21, 2017; Accepted September 7, 2017

ZnO nanostructures with different morphologies successfully were synthesized from a hydrozincite ((Zn)₅(CO₃)₂(OH)₆) precursor under hydrothermal conditions and were examined by means of scanning electron microscopy (SEM), X-ray diffraction (XRD), and Fourier transform infrared spectroscopy (FT-IR). The effects of the different Cl⁻ sources on the shape and morphology of ZnO and also their reaction times were investigated. It is shown that the addition of NaCl, (cyclohexylazanediy)bis(methylene)diphosphonic acid, C₆H₁₁N(CH₂PO₃H₂)₂ and (H₄L) have a significant impact on the growth rate of ZnO {10 $\bar{1}$ 0} planes and (0001) end plane, that could lead to the formation of ZnO rods, various flower-like hexagonal plates and nanoparticles.

Keywords: Aminodiphosphonate, Crystal morphology, Electron microscopy, Hydrothermal reduction, ZnO nano/microcrystals

INTRODUCTION

Zinc oxide (ZnO) nanostructures have been used in many fields as light-emitting diodes [1], nanolasers [2], field-effect transistors [3], solar cells [4] and gas sensors [5-7]. In addition to the above mentioned applications, ZnO is considered as a promising photocatalytic material in the UV spectral range, thanks to its wide direct band gap (3.37 eV), high excitation binding energy (60 meV), excellent chemical/thermal stability, high transparency and non-toxicity [8-10]. Therefore, it is important to develop a simple method for producing high quality ZnO with uniform morphologies. Among the different methods [11-19], hydrothermal methods have become a popular pathway to synthesizing anisotropic nano/micro structures, *e.g.*, rods, cubes, disks, polyhedrals and multipods. In hydrothermal methods, the starting materials can undergo quite unexpected reactions, which are often accompanied by the formation of versatile morphologies that cannot be accessed through classic procedures. Moreover, the occurrence of many novel reactions can be expected in hydrothermal methods due to their specific physical properties, particularly the homogeneous nucleation, high compressibility and high solvation power [20]. In a typical and popular hydrothermal process, adding of additives such as anions, organic or inorganic compounds, changing of basicity and pH of the reactants are used for controlling ZnO's morphology. For example, Wang

et al. synthesized ZnO particles with controllable shape through a cetyltrimethylammonium bromide (CTAB)-assisted hydrothermal method²¹. Yogamalar et al. prepared various shapes of ZnO through a poly-ethylene glycol (PEG 4000)-assisted hydrothermal method [22]. Lu et al. used monoethanolamine (MEA), diethanolamine (DEA), triethanolamine (TEA) and NH₄OH as the alkaline sources to obtain ZnO particles via the hydrothermal process [23]. Sun et al. selected TEA as alkaline sources to synthesize flower-like ZnO through the hydrothermal method [24]. Jang et al. studied the morphology change of ZnO nanostructures with different pH in the hydrothermal process [25].

However, the present work presents the result of the efforts to synthesize various morphologies of ZnO by use of a simple hydrothermal method with hydrozincite ((Zn)₅(CO₃)₂(OH)₆) as precursor. well-defined single-crystalline ZnO nano/micro-scale structures, such as rods, different flower-like, hexagonal plates and nanoparticles were obtained by adding simple salt (NaCl) or one of aminodiphosphonate derivatives (cyclohexylazanediy)-bis(methylene)-diphosphonic acid, C₆H₁₁N(CH₂PO₃H₂)₂, (H₄L)) for controlling the growth of different crystal planes. H₄L is a strong tetradentate chelating agent for zinc ions with a higher stability constant than other complexing agents such as hydroxyl groups. It is examined that H₄L was utilized as a capping and complexing agent for production of zinc oxide by zinc ions, although the phosphonate derivatives have been widely used for fabrication of the inorganic-organic hybrid materials [26-29]. The selected samples were characterized by scanning electron

* To whom all correspondence should be sent:
E-mail: sjamehbozorgi@gmail.com

microscopy (SEM), X-ray diffraction (XRD) and Fourier transform infrared spectroscopy (FT-IR).

EXPERIMENTAL

Materials and methods

The white dry powder of hydrozincite was supplied by Abroon Azma Company from domestic sources in Iran. Other required reagent grade Chemicals were obtained from commercial sources and used without any further purification. Deionized water was used in the experiments.

Cyclohexylazanediylobis(methylene)diphosphonic acid, $C_6H_{11}N(CH_2PO_3H_2)_2$, (H_4L) was prepared according to Moedritzer-Irani synthesis [30, 31]. A mixture of cyclohexylamine (0.5 mol) and crystalline phosphoric acid (82 g, 1 mole) was dissolved in 100 mL of water and 100 mL of concentrated HCl was treated with 2 moles of aqueous 37% formaldehyde solution (100% excess) and was heated to reflux in a three-necked flask. The resultant solution was kept at room temperature. White crystals of the product were obtained after 3 days. Yield: 86%, m.p.: 260 8C. Anal. calc. for $C_8H_{19}NO_6P_2$ (278.19): C 33.46, H 6.67, N 4.88; found: C 33.48, H 6.70, N 4.48. IR (KBr)/ cm^{-1} : 3453

(bw), 2965 (m), 2875 (w), 2569 (bw), 2283 (bw), 1458 (w), 1228 (s), 1173 (s). 1H NMR (D_2O , ppm): d = 1.05–1.97 (m, 10H, ring CH_2), 3.42 (d, $^2J_{PH} = 13$, 4H, NCH_2P), 3.70 (m, 1H, NCH). ^{13}C NMR (D_2O , ppm): d = 24.80 (s), 24.84 (s), 26.62 (s), 49.11 (d, $^1J_{PC} = 140.71$, NCH_2P), 66.81(s).

Synthesis of nano zinc oxide

ZnO nanoparticles were prepared by the hydrothermal reaction of hydrozincite ($((Zn)_5(CO_3)_2(OH)_6)$) and sodium hydroxide in a stainless steel autoclave at autogenous pressure. In a typical synthesis of nano zinc oxide, hydrozincite was dissolved in 10 ml deionized water and then pH of the solution was adjusted to 14 by adding NaOH (10 M) solution. The resulting slurry was then transferred to a Teflon-lined stainless steel autoclave with an inner volume of 25 mL and was heated up to 170°C for 20 minutes in an oven. Later on, the autoclave cooled down naturally to the room temperature. The resulting white powder was filtered and dried in air after being washed three times with methanol and deionized water. The list of the major products is given in Table 1.

Table 1. Products obtained when the reactants were added using different procedures.

Sample No	Hydrozincite ($mmolL^{-1}$)	$H_4L(mmoll^{-1})$	NaCl(M)	Time(hour)	Figure
1	18	-	-	20	1
2	18	-	0.1	20	2a
3	18	-	0.3	20	2b
4	18	-	0.4	20	2c
5	18	-	0.8	20	2d
6	18	17	-	20	3a
7	18	17	-	60	3b

Characterization

X-ray diffractions (XRD) were done by using GNR MPD3000, powder X-ray diffraction ($Cu K_{\alpha} = 1.5406 \text{ \AA}$). The scanning electron microscopy (SEM) images were obtained on a TESCAN SEM instrument equipped with an X-ray energy dispersive detector. FTIR spectra were measured from KBr disks through NICOLET IR 100 Spectrophotometer.

RESULTS AND DISCUSSION

SEM Analysis

The morphology and the size of the ZnO crystals were examined by SEM. Figures 1-3 present the SEM images of the synthesized ZnO samples. It could be observed that the adjustment of the reaction conditions would lead to the formation of different shapes and morphologies. As shown in Figure 1, the product was composed of the hexagonal rods with the length in 4-30 μm . To get expected result, the reaction was lasted 20

hours at 170°C with 18 mmolL⁻¹ concentration of hydrozincite. Moreover, some of the ZnO nanorods tend to self-assemble 3D (three-dimensional) flower-like ZnO bundles. Every bundle is composed of tightly packed submicro-scale hexagonal rods with a diameter of 200–700 nm and the length of 4–8 μm forming radiating structures.

Different salt concentrations were tested to reveal the effect of salt on the final morphology of the products. Dissolving of 0.1 M NaCl in a mixture of reaction led to formation of nanorod-based flowerlike architectures with a diameter of 2 μm (Fig.2a). The low-magnification SEM image (the inset in Fig. 2a) showed that the nanorods tend to attach together and assemble into 3D flowerlike architectures. Each rod was about 1 μm in length and 200 nm in diameter. In addition to nanorods, irregularly oriented ZnO particles could also be observed, suggesting that the ZnO nanorods might be formed by the assembly of the small ZnO nanoparticles during the heat-treatment process. Interestingly, an increase in NaCl concentration to 0.3 M, resulted in a product which was completely

composed to hexagonal ZnO nanoplates with an average diameter of 50 nm and lateral dimension of up to 300 nm (Fig. 2b).

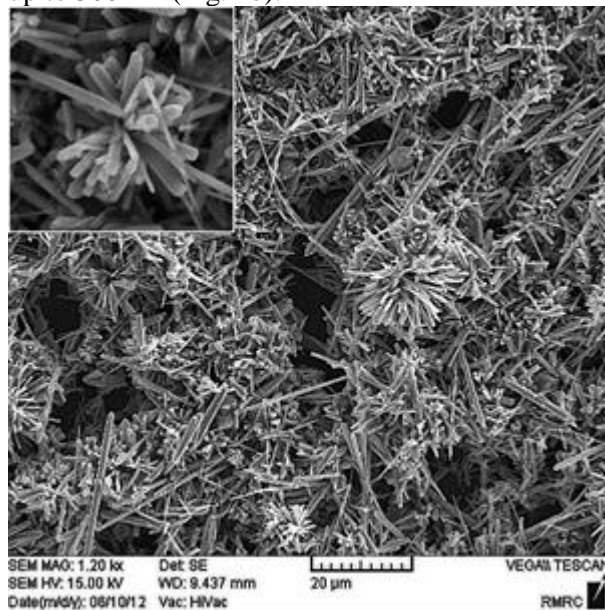


Figure 1. SEM images of ZnO crystals prepared using hydrozincite (18 mmolL⁻¹) by hydrothermal method, temperature: 170°C; time: 20 h.

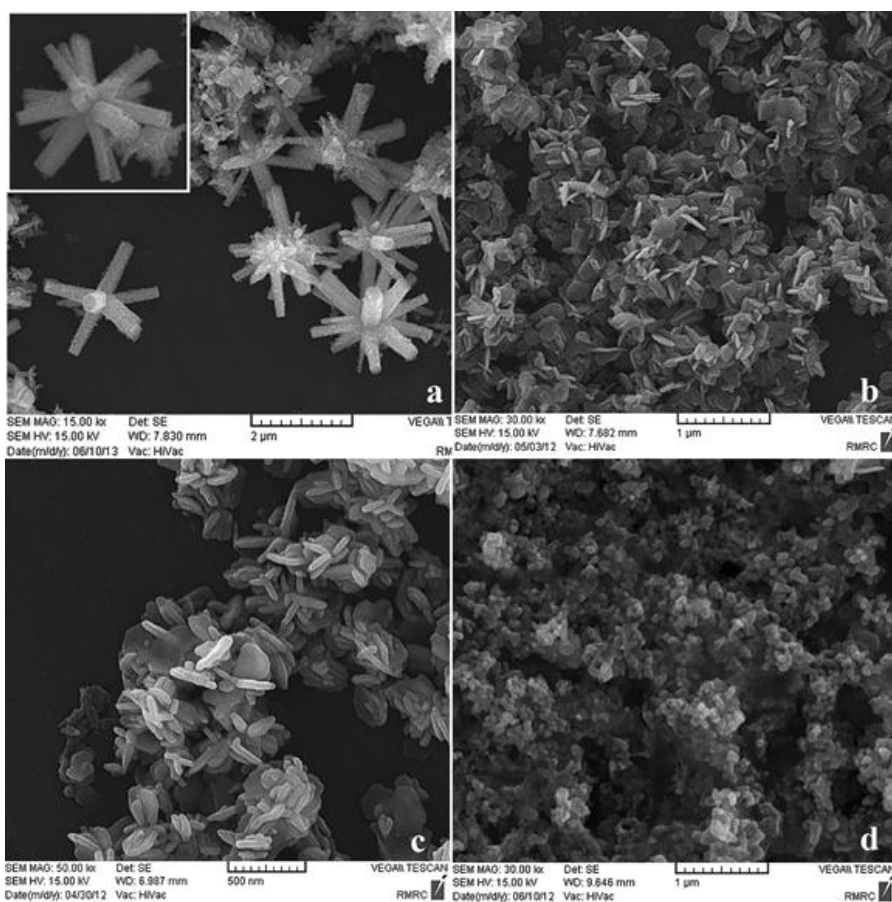


Figure 2. Effect of NaCl concentration on the ZnO growth habit changes using hydrozincite (18 mmolL⁻¹) at 170°C; for 20 h: (a) 0.1 M, (b) 0.3M, (c) 0.4M and (d) 0.8M.

Increasing of NaCl concentration to 0.4 M led to a product that contained the same plate-like crystals and small rice-like nanocrystals with 150- 250 nm in length and 30 nm in diameter (Fig.2c).

We noticed that further increasing of NaCl concentration to 0.8 M also yielded small nanoparticles less than 100 nm (as displayed in Fig. 2d). These results demonstrate that, Cl⁻ concentration is a key factor for controlling the morphology evolution of ZnO micro/nano-architectures. Fig. 3 shows the crystal morphologies

produced at different reaction times when concentration of hydrozincite and H₄L were 18 and 17 mmolL⁻¹, respectively at 170°C within 20 hours test duration. The product consisted of individual flower-like ZnO nanostructure with a size of about 1 μm and undefined quantity of leaves several hundred nanometre in size (Fig. 3a). Finally, well-defined 3D flower-like micro-structures composed of more and larger leaves with the length of in 1 μm were obtained after extending the reaction time to 60 hours (Fig. 3b).

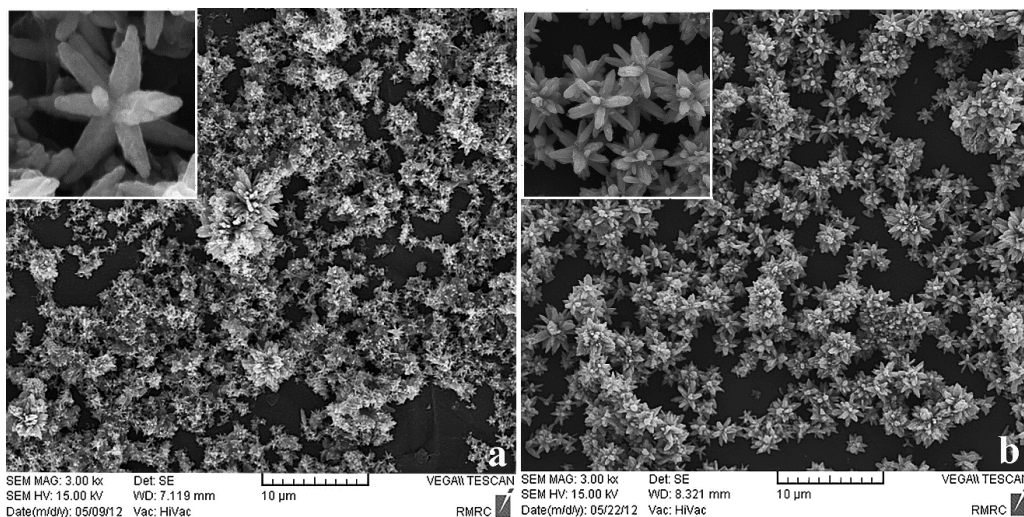


Figure 3. Effect of reaction time on the ZnO growth habit changes using hydrozincite (18 mmolL⁻¹) and H₄L (17 mmolL⁻¹) at 170° C: (a) 20 h and (b) 60 h.

XRD Analysis

XRD patterns of the ZnO nano/micro-scale structures with different crystal shapes are shown in Fig. 4. All diffraction peaks could be indexed to wurtzite (hexagonal) structured ZnO (space group P63mc) with cell parameters $a = 3.249 \text{ \AA}$ and $c = 5.206 \text{ \AA}$, which reflects a good agreement with the literature values (JCPDS card, no. 36-1451). No

characteristic peaks of other impurities such as Zn(OH)₂ were detected in the patterns and it could be indicated that only single-phase ZnO samples were formed. The sharp diffraction peaks showed the good crystallinity of the synthesized ZnO products. Based on the XRD data, we could illustrate the texture effect of the anisotropic morphology and orientation on the relative intensity of the diffraction peak.

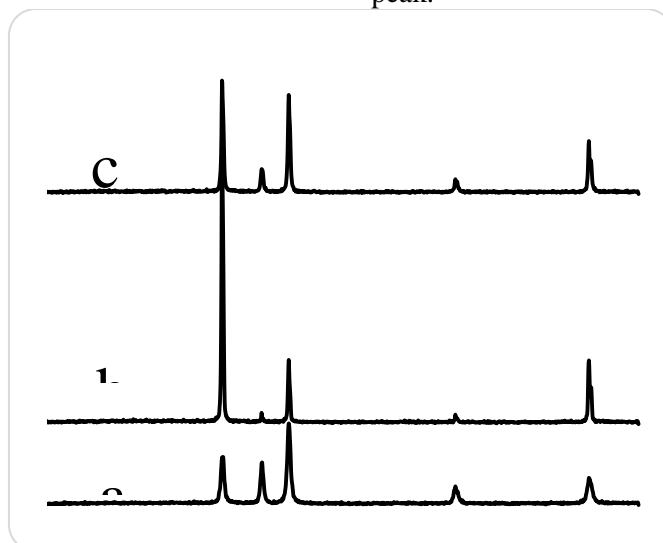


Figure 4. The typical XRD patterns of ZnO (a) rod, (b) plate and (c) flower-like.

The existence of ZnO rods in sample 1 (Figure 1) is related to the X-ray incident beam. More amounts of (0002) planes cause the higher intensity of its peak in sample 1 than the other samples (Figure 4a). The XRD pattern of the plate-shaped ZnO (Figures 2b and 2c) indicated that the $(10\bar{1}0)$ diffraction peak was unusually large compared to (0002) peak. Interestingly, one can find that the diffraction intensity of $(10\bar{1}0)$ peak of the flower-like ZnO (Figures 2a, 3a and 3b) was higher than the standard pattern of hexagonal ZnO (JCPDS No. 36-1451). This phenomenon could be credited to the special orientation growth behaviour.

The facet selective growth of micro/nano-architectures was determined by the energetically favourable growth principle, which might be helpful to understand the growth mechanism of different morphology of ZnO. In basic solutions, the predominantly existing soluble zinc species was $[\text{Zn}(\text{OH})_4]^{2-}$, which was considered to be the growth unit of ZnO. As a result, it can be claimed that the adsorption of $[\text{Zn}(\text{OH})_4]^{2-}$ on different energetically favourable growth planes determined the morphology evolution. The structured wurtzite ZnO crystal schematically described as a number of alternating flat composite of four-fold coordinated O_2 and Zn^{2+} ions, stacked alternately along the c-axis¹⁷. Because of the special crystal structure of ZnO a rapid crystal growth along (1000) direction for ZnO was expected. In the aqueous solution, the anisotropic growth of ZnO crystals, along (0001) direction, progressed through the adsorption of the $[\text{Zn}(\text{OH})_4]^{2-}$ units onto the (0002) plane which resulted in a fast growth along the (0001) direction. Therefore, the intrinsic habit of a single crystal ZnO was elongated rods along the c-axis or the hierarchical nanostructures self-assembled with the rod.

The second energetically favourable growth of $(10\bar{1}0)$ plane indicates the lateral preferred growth of $\{10\bar{1}0\}$ planes of rod-like ZnO. Consequently, rod-like ZnO bounded by (0002), $(10\bar{1}0)$, $(01\bar{1}0)$, $(\bar{1}100)$, $(\bar{1}010)$, $(1\bar{1}00)$ and $(0\bar{1}10)$ planes is achieved, which exhibits hexagonal sectional morphology because of the 120° internal angle between $\{10\bar{1}0\}$ planes.

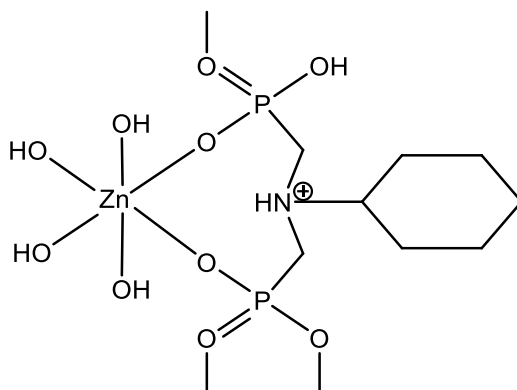
Many experimental factors, such as adsorption of charged particles on some surface of polar ZnO crystals, structure-directing agents, reaction time and substrate play important roles for the morphology evolution of ZnO. Lu et al. found that the addition of KCl, NaCl, and ethylenediamine and

the hydrolysis of hexamethylenetetramine lead to the formation of highly oriented ZnO rods, flower-like ZnO bundles, nanowire arrays or hexagonal plates [32]. Wang et al. found that many ions in the reaction solution could adsorb on the surface of ZnO nuclei and could have great effects on the coarsening rate [33].

Based on our experiments, it was found that the morphology and size of ZnO crystals markedly depends on the NaCl concentration. The preferential adsorption of Cl^- on the (0002) planes can prevent growth along the c-axis, leading to preferential growth on the $(10\bar{1}0)$ planes.

In the absence of Cl^- ions, the product is sub-micrometers rods with the length in 4-30 μm and some flower-like ZnO bundles composed of hexagonal rods in length 4-8 μm (sample 1). When the Cl^- concentration is 0.1 M, restricted growth along c-axis leads to “nanorod-based flowerlike” architectures. In this case, the average length of ZnO rods decreases to about 1 μm (sample 2). When the Cl^- concentration is increased, this ion completely adsorb on the positively charged (0002) plane, leading to the formation of nanoplates (sample 3). It should be noted that in the high NaCl concentration, too much Cl^- exists in sample, which covers all the planes for the nucleation and growth of ZnO. As a result, ZnO loses its preferred growth of (0002) and $\{10\bar{1}0\}$ planes, leading to disordered growth and the formation of small rice-like particles (sample 4) and nanoparticles (sample 5).

In this study H_4L was used as both a structure directing agent and a capping agent to produce ZnO nanoparticles (scheme 1). During the hydrothermal treatment, the zinc- H_4L complex was formed and free Zn^{2+} decreased³¹. In this case, there was not enough $[\text{Zn}(\text{OH})_4]^{2-}$ for the nucleation and growth of ZnO, just resulting in further restricted growth along the c-axis and formation of nanoleaves instead on nanorods. In order to minimize the system energy, the formed ZnO nanoleaves self-assemble to 3D flower-like ZnO with the size of about 1 μm (sample 6). When the hydrothermal treatment time was increased, more and larger nanoleaves grew and the shapes of the flower-like ZnO were further developed (sample 7). Therefore, it can be concluded that further increase in the hydrothermal treatment time makes the diameters of the nanoleaves more uniform and the well-defined 3D flower-like microstructures produced in accordance with the Ostwald ripening mechanism.



Scheme 1. H₄L as both a structure directing agent and a capping agent

In addition, H₄L was used as capping agent to passivate the surface of ZnO nanoparticles and stabilize nanoparticles owing to the coordination of O atoms of –PO₃ groups with Zn atoms at the surface of ZnO nanoparticles.

FTIR Study

FTIR spectroscopy was used to probe the chemical composition of the surface of the ZnO particles of sample 7 and the local molecular environment of the capping agents on the ZnO crystals. The following assignments are based on published values for similar compounds [14].

In the H₄L spectrum (Figure 5a), the broad and strong bands in 3100–3600 cm⁻¹ range and weaker absorptions of δ(H–O–H) in 1695–1633 cm⁻¹ region are assigned to OH stretching vibrations of coordinated water molecules. The strong band at 2956 cm⁻¹ and the small one at 2918 cm⁻¹ are typical of C–H stretching vibrations of the CH₂ groups and the sharp band at 1457 cm⁻¹ is due to the CH₂

deformation vibration. In the spectrum of ZnO crystals of sample 7 (Figure 5b), all these peaks nearly maintain their position. However, IR spectrum of H₄L shows a series of strong bands in the 1195–919 cm⁻¹ range, are attributed to the stretching vibrations of –PO₃ groups which are characteristic of hydrogen phosphonate groups. In the ZnO crystals, these peaks appear in the 1043 cm⁻¹. These shifts might be attributed to the interaction between Zn and –PO₃ group through the partial coordination of the lone pair electrons on the O atom. Furthermore, in H₄L spectrum, the two bands observed in 2850–2650 and 2350–2100 cm⁻¹ regions, are likely due to ν(P–OH) and δ(P–O–H) respectively, which are characteristic of hydrogen phosphonate groups. The δ(P–O–H) band disappeared in the ZnO crystals spectrum, giving evidence for the interaction between oxygen of –P–O and Zn atoms on ZnO crystals.

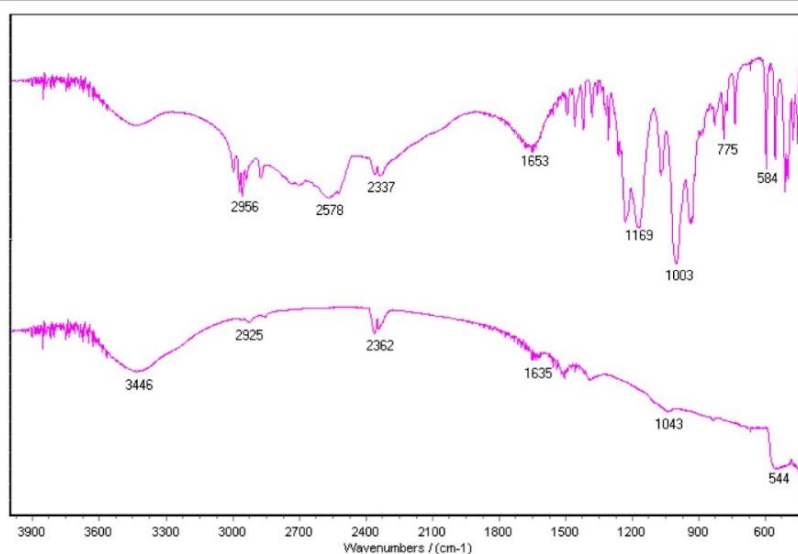


Figure 5. FTIR spectra of (a) synthesized H₄L and (b) ZnO flower-like crystals obtained from sample 7.

EDS Analysis

Besides IR spectroscopy, the presence of capping agent on the surface of synthesized ZnO crystals was confirmed by EDS analysis. The EDS analysis of the flower-like product (sample 7, Figure 6) demonstrated that Zn and O were their main elements, indicating the formation of ZnO in our

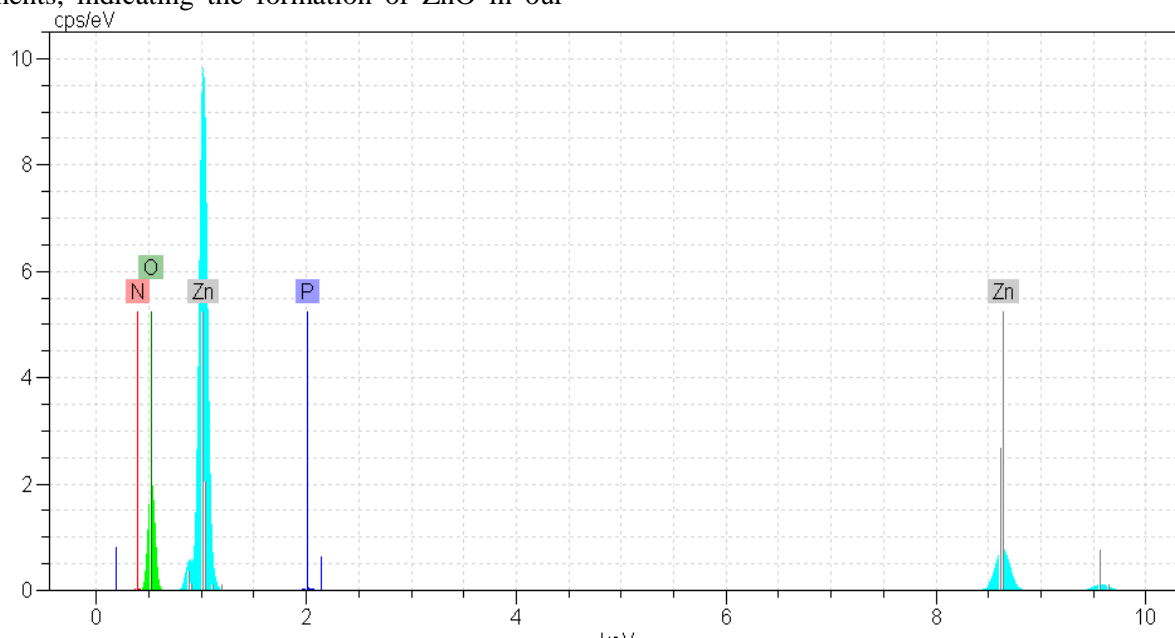


Figure 6. EDS analysis of ZnO flower-like crystals obtained from sample 7.

CONCLUSION

Different morphology of ZnO nano/micro structures have been synthesized via a simple hydrothermal route with hydrozincite $((\text{Zn})_5(\text{CO}_3)_2(\text{OH})_6)$ as precursor. It was demonstrated that the addition of NaCl and cyclohexylazanediybis(methylene)diphosphonic acid, (H₄L) lead to differences in growth rates of ZnO $\{10\bar{1}0\}$ planes and (0002) end planes, respectively. It could also result in the formation of ZnO rods, flower-like ZnO plates and nanoparticles. The FTIR spectroscopy and EDS analysis established the protection of ZnO flower-like crystals by H₄L in the hydrothermal treatment.

REFERENCES

1. Q. Qiao, B. H. Li, C. X. Shan, J. S. Liu, J. Yu, X. H. Xie, Z. Z. Zhang, T. B. Ji, Y. Jia, D. Z. Shen, *Mater. Lett.*, **74**, 104 (2012).
2. H. Zhou, M. Wissinger, J. Fallert, R. Hauschild, F. Stelzl, C. Klingshirn, H. Kalt, *Appl. Phys. Lett.*, **91**, 181112 (2007).
3. P. Atanasova, D. Rothenstein, J. J. Schneider, R. C. Hoffmann, S. Dilfer, S. Eiben, C. Wege, H. Jeske, *Adv. Mater.*, **23**, 4918 (2011).
4. J. J. Wu, Y. R. Chen, W. P. Liao, C. T. Wu and C. Y. Chen, *ACS Nano*, **4**, 5679 (2010).
5. N. F. Hamedani, A. R. Mahjoub, A. AKhodadadi and Y. Mortazavi, *Sens. Actuators. B*, **156**, 737 (2011).
6. Y. Zhang, J. Q. Xu, P. C. Xu, Y. H. Zhu, X. D. Chen and W. J. Yu, *Nanotechnol.* **21**, 285501 (2010).
7. U. Ozgur, Y. I. Alivov, C. Liu, A. Teke, M. A. Reshchikov, S. Dogan, V. Avrutin, S. J. Cho, H. Morkoc, *J. Appl. Phys.*, **98**, 041301 (2005).
8. Y. K. Su, S. M. Peng, L. W. Ji, C. Z. Wu, W. B. Cheng, C. H. Liu, *Langmuir*, **26**, 603 (2010).
9. B. S. Ong, C. S. Li, Y. N. Li, Y. L. Wu, R. Loutfy, *J. Am. Chem. Soc.*, **1299**, 2750 (2007).
10. L. Schmidt-Mende, J. L. MacManus-Driscoll, *Mater. Today.*, **10**, 40 (2007).
11. S. Cho, J. Jang, S. Jung, B. R. Lee, E. Oh, K. Lee, *Langmuir*, **25**, 3825 (2009).
12. J. J. Wu, Y. R. Chen, W. P. Liao, C. T. Wu, C. Y. Chen, *ACS Nano.*, **4**, 5679 (2010).
13. D. Choi, M. Y. Choi, W. M. Choi, H. J. Shin, H. K. Park, J. S. Seo, J. Park, S. M. Yoon, S. J. Chae, Y. H. Lee, S. W. Kim, J. Y. Choi, S. Y. Lee, J. M. Kim, *Adv. Mater.*, **22**, 2187 (2010).
14. M. J. S. Spencer, I. Yarovsky, *J. Phys. Chem. C.*, **11**, 410881 (2010).
15. Z. Han, L. Liao, Y. Wu, H. Pan, S. Shen, J. Chen, *J. Hazard. Mater.*, **217**, 100 (2012).
16. C. Zhu, B. Lu, Q. Su, E. Xie, W. Lan, *Nanoscale*, **4**, 3060 (2012).
17. Z. R. Tian, J. A. Voigt, J. Liu, B. Mckenzie, M. J. Mcdermott, M. A. Rodriguez, H. Konishi, H. F. Xu, *Nat. Mater.*, **2**, 821 (2003).

experiment. The molar ratio of Zn and O is very near to stoichiometric molar ratio of ZnO. Moreover, N and P element appear in the EDS spectra.

These observations can be attributed to the constraint of the capping molecular motions on the surface of ZnO crystals.

18. R. Ianos, I. Lazau, C. Pacurariu, P. Sfirloaga, *Mater. Chem. Phys.*, **129**, 881 (2011).
19. D. Zaouk, Y. Zaatat, R. Asmar, J. Jabbour, *J. Microelectromech. Syst.*, **37**, 1276 (2006).
20. P. Chen, G. Lee, S. Anandan, J. Wu, *J. Mater. Sci. Eng. B.*, **177**, 190 (2012).
21. Y.X. Wang, J. Sun, X.Y. Fan, X. Yu, *Ceram. Int.*, **37**, 3431 (2011).
22. N. R. Yogamalar, A. C. Bose, *J. Solid State Chem.*, **184**, 12 (2011).
23. C. Lu, Y. Lai, R. B. Kale, *J. Alloys Compd.* **477**, 523 (2009).
24. L. Sun, R. Shao, Z. Chen, L. Tang, Y. Dai, J. Ding, *Appl. Surf. Sci.*, **258**, 5455 (2012).
25. J. Jang, S. Kim, H. Choi, J. Kim, W. Jung, *Mater. Chem. Phys.*, **113**, (15) 389 (2009).
26. A. Rabenau, *Angew. Chem. Int. Ed.*, **24**, 1026 (1985).
27. Y. Liu, Y. Chu, Y. Zhuo, L. Dong, L. Li, M. Li, *Adv. Funct. Mater.*, **17**, 933 (2007).
28. X. Zhang, D. Zhang, X. Ni, H. Zheng, *Solid State Commun.*, **139**, 412 (2006).
29. C. Jiang, W. Zhan, Y. Liu, Y. Qian, *Cryst. Growth. Des.*, **6**, 1440 (2006).
30. K. Moedritzer, R.R. Irani, *J. Org. Chem.*, **31**, 1603 (1966).
31. S. Dehghanpour, A. Mahmoudi, F. Esbati, S.Hadian Rasanani, *Mater. Res. Bull.*, **47**, 2126 (2012).
32. F. Xu, Y. Lu, Y. Xie, Y. Liu, *Mater. Des.*, **30**, 1704 (2009).
33. Z. Wang, X.F. Qian, J. Yin, Z. K. Zhu, *Langmuir*, **20**, 3441 (2004).
34. S. Dehghanpour, A. Mahmoudi, M. Mirsaeed-Ghazi, N. Bazvand, S. Shadpour, A. Nemat, *Powder Technol.*, **246**, 148 (2013).